Hindawi
Shock and Vibration
Volume 2023, Article ID 5054971, 10 pages
https://doi.org/10.1155/2023/5054971

Research Article

Propagation Characteristics of Explosion Wave and Explosion Gas in Blast-Hole

Jinjing Zuo,[1] **Renshu Yang**,[1,2] **and Quanmin Xie**[3]

[1]*School of Civil and Environment Engineering, University of Science and Technology Beijing, Beijing 100083, China*
[2]*State Key Laboratory for Geomechanics and Deep Underground Engineering (Beijing), Beijing 100083, China*
[3]*State Key Laboratory of Precision Blasting, Jianghan University, Wuhan 430056, China*

Correspondence should be addressed to Jinjing Zuo; cumtbzjj@163.com

Received 17 March 2023; Revised 3 June 2023; Accepted 8 June 2023; Published 13 July 2023

Academic Editor: S. Mahdi S. Kolbadi

In order to explore the propagation characteristics of explosion wave and gas in blast-hole, design a model to simulate blast-hole charge in the laboratory, adopted a high-speed schlieren experiment system used to study the evolution characteristics of explosion wave field under two kinds of charge structures. The results showed similar explosion wave velocities for the two cartridges, the explosion wave was reflected when it reaches the hole wall, and the reflected wave velocity was lower than an incident wave. The explosion gas tends to cluster and spread in a cutting direction, resulting in intensified destruction in that direction. The explosion wave first emerges in the direction of the slits, and then moves towards the blast-hole walls, which indicates that the explosion energy can be accumulated in the slit direction and cause directional destruction of the medium. To study this process in detail, establish numerical model for the propagation of explosive in the hole. The results indicated that the detonation products first come out in the direction of the slits and then go around towards other areas in a distribution that is consistent with the observations by high-speed schlieren photography.

1. Introduction

The structure of a cutting seam cartridge makes a significant contribution in delivering directional explosive cracks. For this reason, many studies have examined the principles of the cutting seam cartridge in rock blasting. As early as the 1970s, it has been proposed a method to create directional cracks in rock using axially slitted tubular cartridges in blast-holes. Fourney et al. [1, 2] conducted a series of explosion experiments was performed with slitted tubular cartridges, which showed that cracks can be controlled even under explosive conditions. Cho et al. [3] performed model tests and numerical simulations, observed significantly directed blast-hole grooves that were conducive to the formation of a flat crack surface. Isakov [4] proposed a loading method in which an axially grooved solid shell was positioned along the blast-hole wall; experiments revealed that the crack distribution caused by an explosion may be influenced by shell strength, shell thickness, and the initial burst pressure of the cavity. The caustic specks at the crack tip can be observed in the dynamic caustic experiment system, and the crack propagation velocity and stress intensity factor can be calculated [5, 6]. Yang et al. [7, 8] studied the directional crack characteristics of a cutting seam cartridge, and the transmission mechanism of the explosion wave of the cutting seam cartridge with different uncoupling coefficients. Yue et al. [9–11] analysed the interaction between cracks for a double-hole directional crack-controlled explosive using the caustic method, also studied the application of the cutting seam cartridge. Guo et al. [12] studied the change of the mechanical parameters of the crack tip created by explosive when the crack approaches a hole defect. Yang and Wang [13, 14] studied cracks by the cutting seam cartridges of different structures using the caustic method and numerical analysis software. The experiments found that the cutting seam cartridge can cause directional cracks in the medium. Ma and An [15] used the *J-H* material

model of LS-DYNA numerical simulation software, studied the explosion effect under different groove angles in grooved explosive.

The high-speed schlieren experiment system can monitor the density change of the air field under disturbance [16, 17]. Yang et al. [18, 19] adopted this device and studied the evolution of an explosive wave field in an exposed air medium. Zuo et al. [20] studied the explosion wave propagation characteristics of cylindrical explosive at different initiation positions, and obtained the included angle range of explosion shock wave incident on the hole wall, revealed the distribution characteristics of explosion cracks in different areas. Ambrosini et al. [21, 22] using background optical directional schlieren technique, solved the visualization of convective heat transfer, improved the accuracy of temperature measurement by using the windowed Fourier transform method. Zhang [23], using high-speed schlieren photography, overpressure measurement, and numerical simulation were applied to study the shock wave propagation of the charge in a pipe with holes, it turns out that the blast wave in the direction of the hole was released more fully.

However, most studies on the explosion wave of a cartridge have been speculative proposals based on explosive theories, and there is a striking lack of comprehensive experimental studies on the explosion wave of a cartridge. The goal of this work was to capture the fine structural features of a cartridge explosion wave during propagation using the high-speed schlieren photography technique. The dynamic changes in the explosion wave and explosion gas in the blast-hole were also recorded using this technique. The differences in transmission between the common structure package and the cutting seam cartridge were compared and analysed. The results from the high-speed schlieren photography and numerical analysis provide insight into the dynamic change in the explosion wave of a cartridge.

2. Experimental Description

2.1. Experimental Details. The experimental loading design included a common cartridge and a cutting seam cartridge. The material of the cutting seam cartridge is stainless steel pipe, the selected explosive is diazodinitrophenol and the dosage is 200 mg. It used a plexiglass tube with a diameter of 40 mm to simulate the blast-hole and studied the transmission characteristics of the explosion wave in the blast-hole. The cartridge was hoisted at the center inside the plexiglass tube. The plexiglass tube and the cartridge were oriented in a direction parallel to the square. Figure 1 shows the common cartridge and cutting seam cartridge for the schlieren experiment.

2.2. Experiment System. Figure 2 shows the structure and schematic diagram of the high-speed schlieren experiment. The composition and testing principle of the experimental system can be referred to the literature [20]. It should be emphasized that the shooting speed of the high-speed camera was 100000 pictures/second during the experiment.

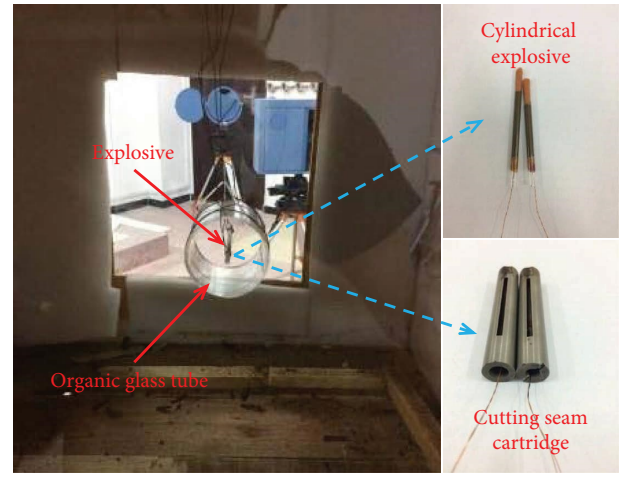

Figure 1: Common cartridge and cutting seam cartridge for the schlieren experiment.

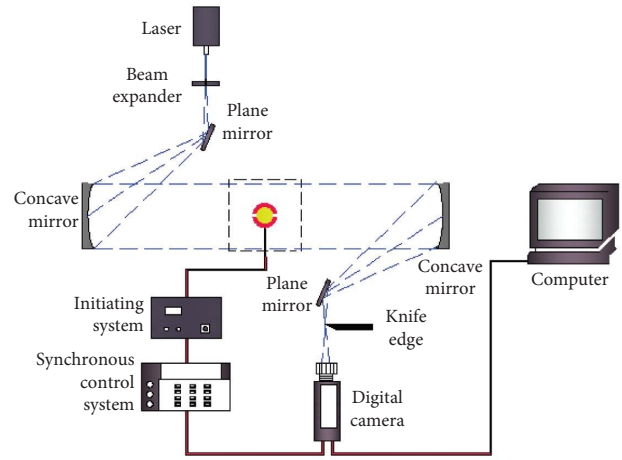

Figure 2: High-speed schlieren experiment system.

3. Experimental Results of Explosion Wave

3.1. Distribution of Explosion Products in the Blast-Hole. Figures 3(a) and 4(a) show the distribution of explosion products in the blast-hole. The distribution of explosion gas in the hole wall can be observed obviously. The experimental results reveal a wide distribution of the explosion products of the common cartridge on the blast-hole. In contrast, the explosion gas of the cutting seam cartridge exhibits a regular distribution on the blast-hole. The explosion products were concentrated in the slit direction, and those in other directions were not concentrated. The explosion gas plays a very important role in rock explosion. The distribution direction of the explosion products also reflects the formation and expansion of the initial crack of the blast-hole wall.

In order to better compare the comparison results under the two charging modes, the distribution range of explosive products in different areas on the blast-hole wall was divided into four quadrants, with 90° as a quadrant, in which the I and III quadrants were the direction of slit cutting of the

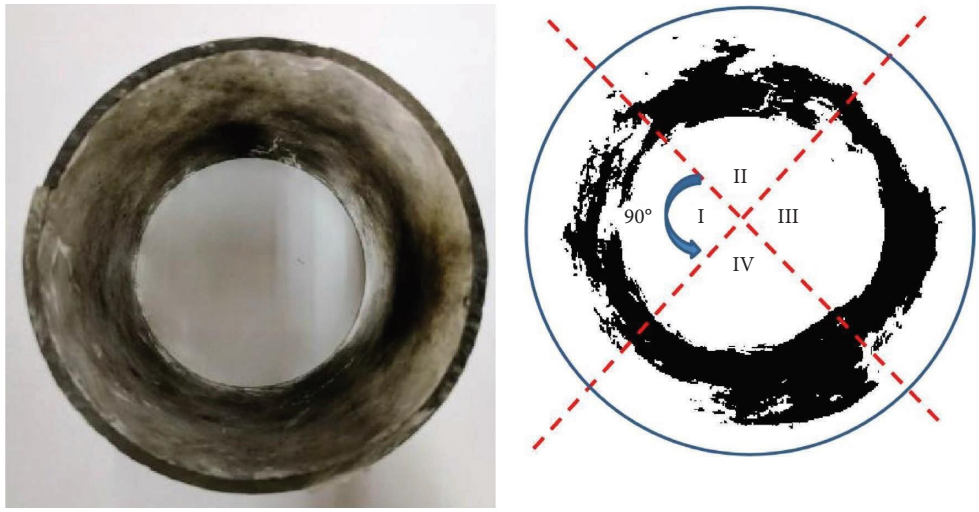

(a) (b)

Figure 3: Distribution of explosive products on the blast-hole of common cartridge (a) experimental result (b) binarization figure.

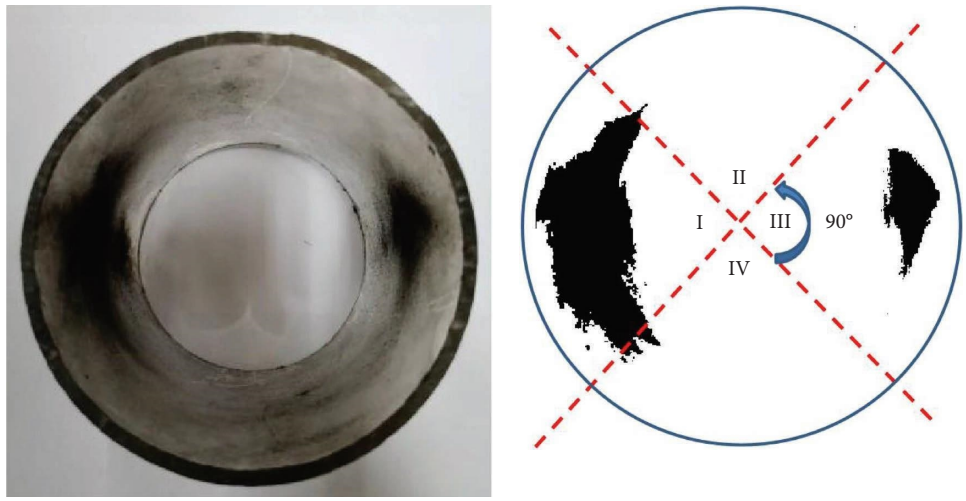

(a) (b)

Figure 4: Distribution of explosive products on the blast-hole of cutting seam cartridge. (a) Experimental result (b) binarization figure.

cartridge package, and the II and IV quadrants were the direction of vertical slit cutting. The results of the four quadrants explosion products were binarized and the results of partition are shown in Figures 3(b) and 4(b).

In order to further analyse the distribution characteristics of explosive products. In this paper, fractal dimension is used to characterize the distribution of explosive products on the blast-hole wall. The box dimension of fractal dimension is used to calculate the possession of explosive products in the selected area. The box dimension is shown in the following formula [24]:

$$\lg N_{\delta_k} = -D \times \lg \delta_k + b. \quad (1)$$

N_{δ_k} is the number of boxes containing divided areas; D is the fractal dimension of regional explosion products. δ_k is the edge length of the small boxes.

Figure 5 shows the fractal dimension results of explosive products in different regions. I and III quadrants were the area which direction of slit, and the II and IV quadrants were area which vertical direction of slit. The distribution of the explosive products of slit charge is relatively concentrated in the I and III quadrants and the fractal dimension was 1.5931 and 1.3785, with an average of 1.4858. However, the distribution of explosion products in II and IV quadrants were less, and the fractal dimension was 0.8202 and 1.0371, with an average value of 0.9287. The average value of explosion products in slit direction was increased by 60.0% compared with that in vertical slit direction. The fractal dimension of common cartridge explosive products in the four quadrants is relatively uniform. Through the above analysis, the cutting seam cartridge has the ability to accumulate explosive products, which indicates that the explosion energy can be accumulated in the slit direction, it can directional destruction of the medium.

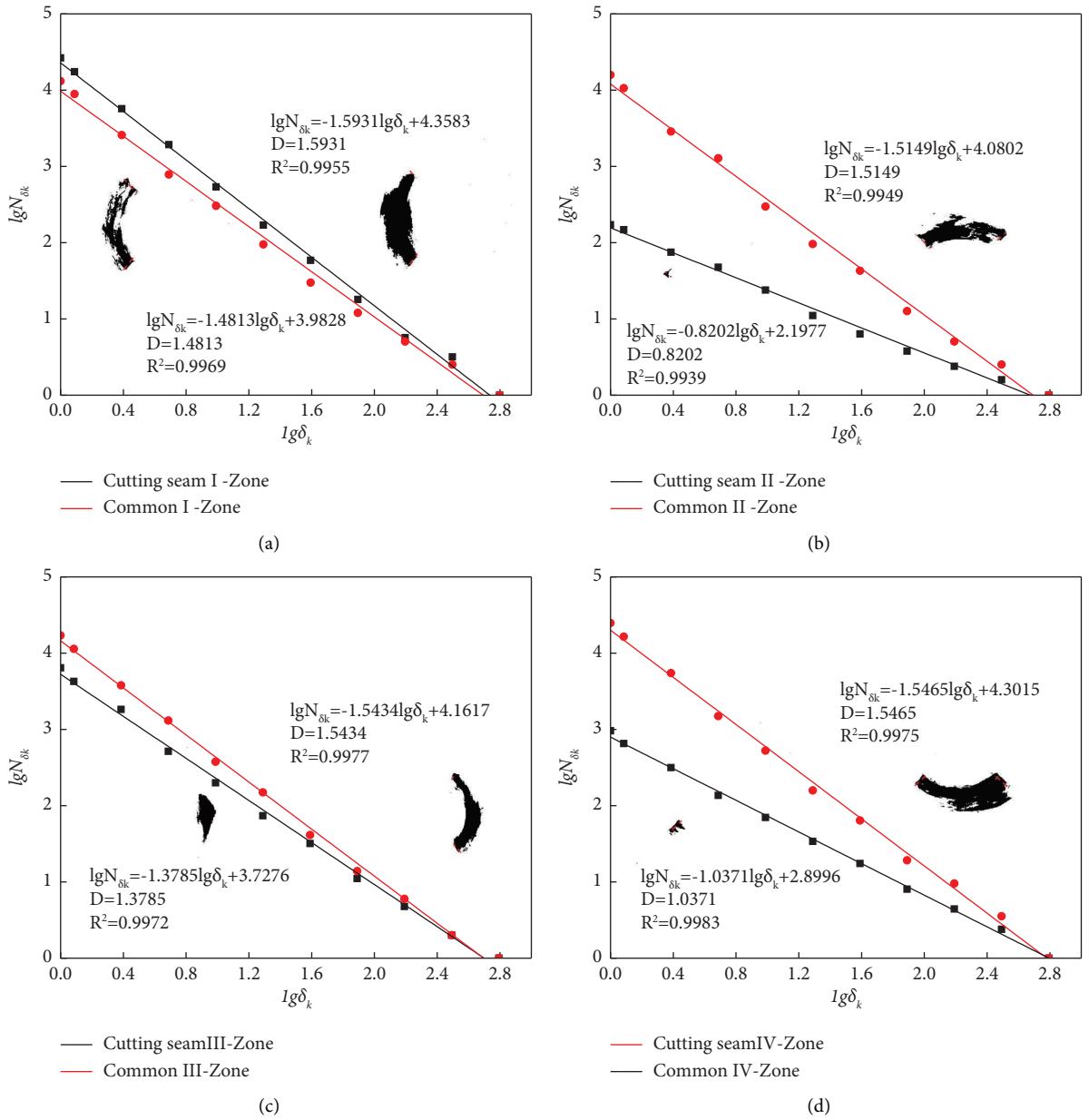

Figure 5: Fractal dimension of explosive product distribution in different quadrants: (a) I quadrants, (b) II quadrants, (c) III quadrants, and (d) IV quadrants.

3.2. The Cutting Seam Cartridge Explosion Wave Process. Figure 6 shows the transmission of the explosion wave and explosion gas for the common cartridge. The explosion wave is obvious at 30 μs, followed by explosion gas. The explosion wave begins to separate from the explosion gas at 40 μs. The explosion wave further develops and the explosion gas travels at a lower velocity at 60 μs. The explosion wave arrives at the blast-hole wall at 110 μs. This explosion wave is gradually reflected and the reflected explosion wave is substantially the same as the shape of the incident explosion wave at 150 μs. The reflected explosion wave further shrinks into the blast-hole until the reflected explosion wave basically disappears at 200 μs. The explosion wave is no longer visible at 380 μs. The explosion gas arrives at the blast-hole wall at 770 μs, but is not evenly distributed.

As shown by the explosion wave transmission of the common cartridge, when the common cartridge is detonated, the explosion wave and the explosion gas initially travel together, but gradually separate, with the explosion wave traveling faster than the explosion gas. Therefore, the explosion wave first reaches the blast-hole wall, and forms a reflected explosion wave that travels inside the blast-hole. However, only one reflected explosion wave can be observed under the experimental conditions. The explosion gas reaches the blast-hole wall after the explosion wave, and its arrival at the blast-hole wall is uneven, so the explosion gas is not significantly reflected.

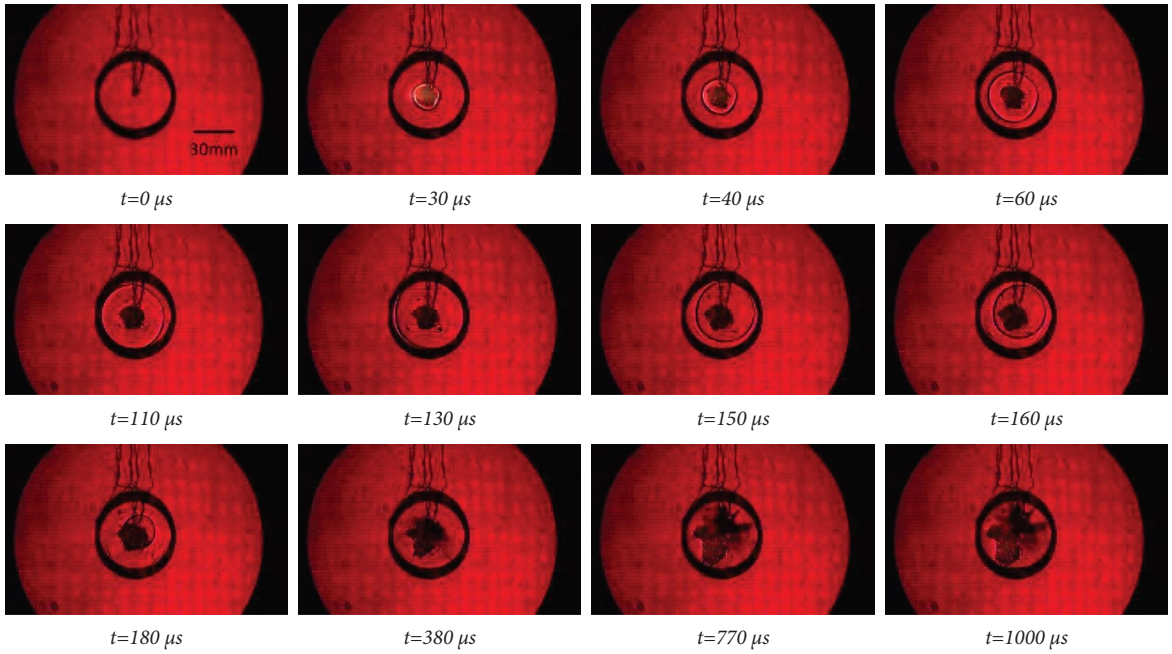

Figure 6: Explosion wave propagation for a common cartridge.

Figure 7 shows the transmission of the explosion wave and explosion gas of the cutting seam cartridge. The explosion wave is obvious to the right and left of the slit at 30 μs, and the explosion wave shape appears like a spindle, and the explosion gas develops from the slit. The explosion wave to the right first arrives at the blast-hole wall at 80 μs, and the explosion gas develops in the slitting direction in the shape of a spindle, and there is no explosion gas expansion of the vertical slit. The reflected explosion wave shrinks inward in a similar elliptical shape at 120 μs. The explosion wave begins to disappear at 180 μs. The explosion gas arrives at blast-hole wall at 310 μs. The explosion wave in the direction of the slit begins to expand around the blast-hole wall at 700 μs, and there is no significant reflection of the explosion gas by the blast-hole wall.

The explosion wave first travels in the direction of the slit, and explosion gas released linearly along the slit direction. The explosion wave travels faster than the explosion gas, and the explosion wave is reflected after reaching the blast-hole wall, forming a reflected explosion wave that shrinks inside the blast-hole.

The cutting seam cartridge and the common cartridge were compared using the schlieren photography technique. The explosion wave first releases energy in the slit direction, and the formed "diversion" of the explosion wave causes the initial damage to the blast-hole wall, further damage occurs due to the quasi-static pressure of the high-pressure explosion gas.

3.3. The Explosion Wave Velocity of the Cartridge. Figure 8(a) shows the change in the expansion velocity of the explosion wave and the explosion gas of the common cartridge. As shown in the figure, the expansion velocity of the explosion gas is lower than that of the explosion wave. Within the 0~120 μs time range, the explosion wave travels from center to the sides, and reflected by the blast-hole wall at 120 μs, forming a reflected explosion wave. There is a velocity peak in this process, in which the reflected explosion wave shrinks inward. Also, the velocity peak explosion wave is far lower than initial explosion wave. The explosion gas velocity is rapidly attenuated within 60 μs, and then the travel velocity of the explosion gas is maintained at about 60 m/s after 60 μs. Figure 8(b) shows the speed change of cutting seam cartridge. The explosion wave is reflected at 80 μs, between 80 and 130 μs, there is a brief zone of velocity increase, and then gradually decrease. Compared with the velocity curve of the common cartridge, the biggest difference lies in the velocity curve of the explosion gas.

4. Numerical Simulation of the Cutting Seam Cartridge Explosion Wave

4.1. Material Model and Parameters. The numerical analysis software adopts AUTODYN [25]. Figure 9 shows the calculation model. Since schlieren experiment can only reflect the propagation characteristics of explosives in the gun hole from the small-scale model experiment in the laboratory, in order to truly reflect the actual conditions, a numerical simulation model in line with the actual construction is established. The explosive diameter is 32 mm, the thickness of the slitting pipe is 2 mm, the incision is 4 mm, the inner diameter of the simulated blast-hole is 45 mm, and the thickness is 3 mm. Several pressure measuring points were arranged in the direction of the slit and vertical slit, of which points 1–5 were in the direction of slit and point 6–10 were in the direction of the vertical slit.

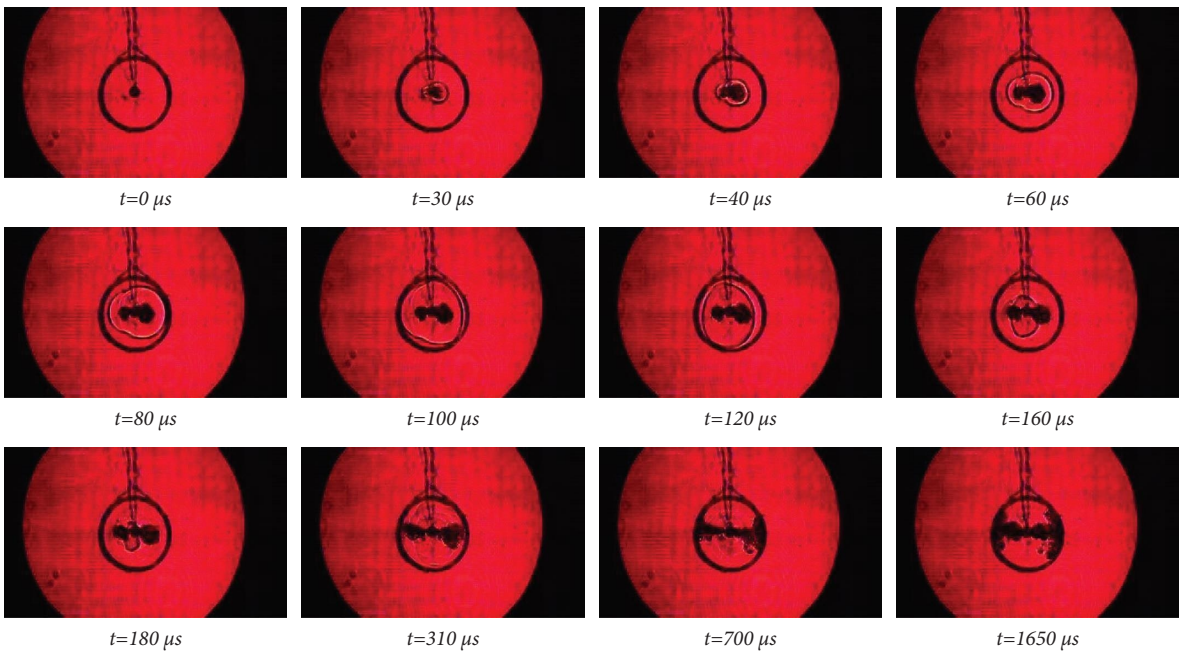

Figure 7: Explosion wave propagation of cutting seam cartridge.

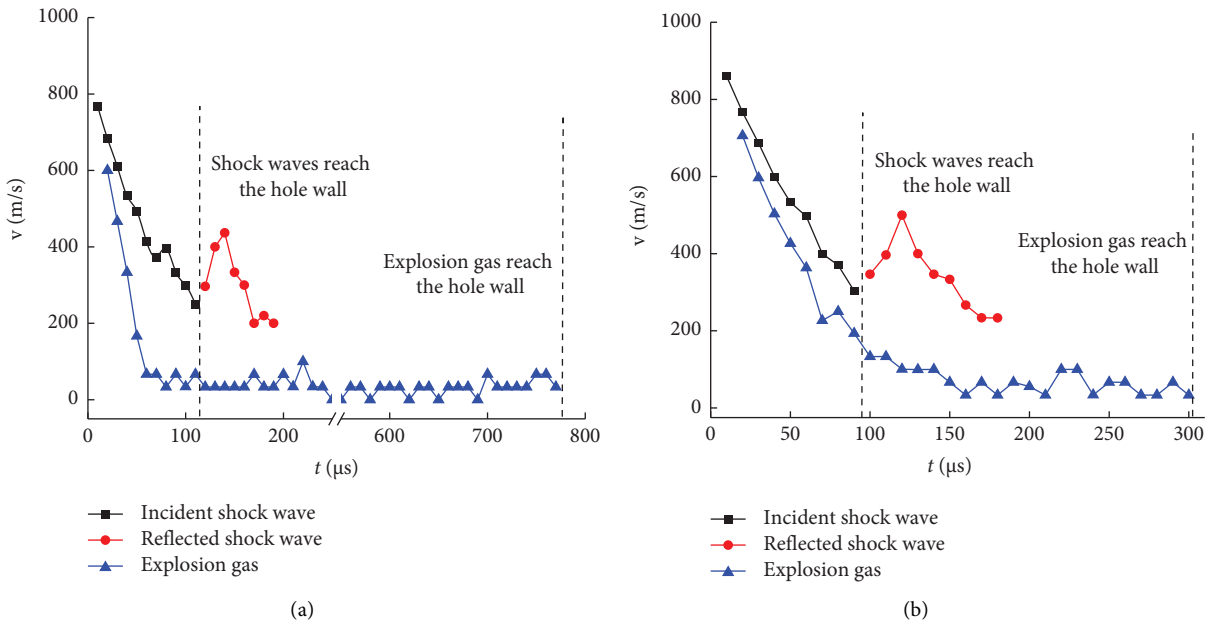

Figure 8: Velocity of the slotted cartridge explosion shock wave and explosion gas speed. (a) Common cartridge and (b) cutting seam cartridge.

Air is modeled as an ideal gas, the explosive used in this calculation is pentaerythritol tetranitrate (PETN), see References [19] for specific parameter settings.

The slitting pipe and blast-hole were made of steel, constitutive model used the Steinberg–Guinan strength model and the Mie–Gruneisen equation of state. The shear modulus G is shown in the following formula [26]:

$$G = G_0\left\{1 + \left[\frac{G_P'}{G_0}\right]\frac{P}{k^{1/2}} + \left[\frac{G_T'}{G_0}\right](T - T_0)\right\}, \quad (2)$$

where T_0 and G_0 are the reference temperature and shear modulus; G_T' and G_P' are constants of selected material; P is the pressure; $k = \rho/\rho_0$. The equation relationship of yield stress Y with effective shaping strain ε^P can be expressed in the following formula:

$$Y = Y_0\left\{1 + \left[\frac{Y_P'}{Y_0}\right]\frac{P}{k^{1/2}} + \left[\frac{G_T'}{G_0}\right](T - T_0)\left(1 + \beta\varepsilon^P\right)^n\right\}, \quad (3)$$

and the following relation is satisfied

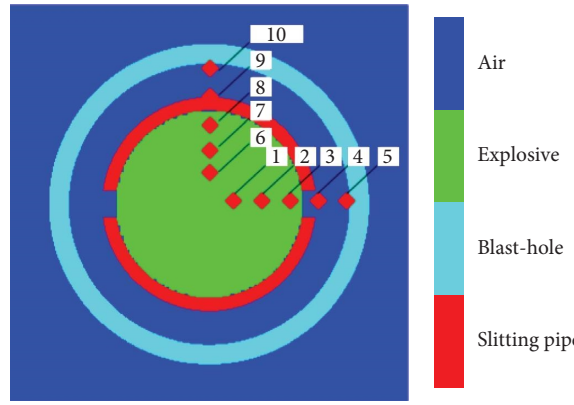

Figure 9: Calculation model.

$$Y_0\left(1+\beta\varepsilon^P\right)^n \le Y_{\max}, \tag{4}$$

where $Y_P^{'}$, β, and n are material constants.

Mie–Gruneisen equation of state, the expression equation shown in the following formula [27]:

$$P = P_r(v) + \frac{\gamma}{v}\left[e - e_r(v)\right], \tag{5}$$

where γ is coefficient number of Gruneisen, v reference volume, e is internal energy, and the expression is $\gamma = \gamma_0/k$, where γ_0 is the reference value, e_r and P_r are the internal energy and pressure, the equation are shown in formulas (6) and (7):

$$P_r(v) = \frac{c_0\rho_0\left(1-\rho_0 v\right)}{\left(1+S\left(\rho_0 v-1\right)^2\right)}, \tag{6}$$

$$P_r(v) = \frac{c_0^2\left(\rho_0 v-1\right)}{2\left(1+S\left(\rho_0 v-1\right)^2\right)}, \tag{7}$$

where c_0 is the speed of sound and S is the material parameter. Specific parameters are shown in Table 1:

4.2. The Explosion Gas Distribution of the Cartridge. Figure 10 shows the explosion gas distribution of the cartridge in the simulated blast-hole. The distribution of explosion gas is highly approximate with the experimental results obtained by high-speed schlieren photography. The explosives considered in the numerical simulation differ from that used in real experiments in terms of explosive type, charge density, and explosion velocity. At the initial explosion stage, the explosion gas first expands in the slitting pipe, and when the explosion gas travels to the outer edge of the slit with a strong pressure wave, eddy currents were generated at both end faces of the outer wall of the slit by explosion wave, making the explosion gas travel in the form of a "*W*." Amid the expansion of the slitting pipe, a large amount of explosion gas bursts out along the slit. The expansion pattern of the explosion gas that reaches the blast-hole wall is highly consistent with that observed in the high-speed schlieren images, and the explosion gas expands along both sides of the blast-hole wall.

4.3. Explosion Wave Transmission in the Blast-Hole. Explosion wave transmission inside the blast-hole is shown in Figure 11. At the beginning, the explosion wave of the explosives in the chemical reaction is the same as that of the explosives without the slitting pipe. The explosion wave mass point is distributed in the form of a sphere. The explosion wave and explosion gas at this point travel together and do not disturb the slitting pipe. The explosion wave interacts with the entire slitting pipe, instantaneously loading the pipe wall and causing a high strain rate, which causes the slitting pipe to expand at a high degree. Amid the expansion, only a small fraction of the explosion gas and explosion wave travel from the slit, as shown in the figure.

The slitting pipe further expands under the impact of the explosion wave. A portion of the explosion wave travels around the outer pipe wall, and a portion of the explosion wave impacts the surrounding medium directly in front of the slit direction. The whole expansion process is similar with the experimental results. The explosion wave interacts with the blast-hole wall, and high pressure is generated at the wall of the blast-hole, allowing the flow of explosion products along the wall.

Figure 12 shows the pressure curve of each monitoring point. Figure 12(a) shows the explosion pressure changes of slit. Points 1–3 were the internal points. The first is caused by the detonation transfer pressure of the explosive when it is detonated, the second by the reflected pressure of the slit tube wall, and the third by the reflected pressure of the blast-hole wall. Point 4 is located outside the cutting seam, and no second fluctuation occurs during the fluctuation process. It can be seen from the pressure curve of point 5 that there were have three fluctuations.

Figure 12(b) shows the explosion pressure changes in the vertical direction of cartridge. Points 6–8 were the internal observation points. Compared with the corresponding pressure points 1–3, the pressure of the first peak is basically the same, but the peak of the reflected pressure in the second is very different, generally higher than the points 1–3 the second peak pressure. The pressure fluctuation of point 9 and point 10 were caused by two parts, one part was caused by explosion gas flows around the blast-hole wall, the other part was caused by the slitting pipe expansion of internal pressure.

Table 1: Physical and mechanical parameters of steel.

ρ_0 (g·cm^{-3})	Y_0 (MPa)	G_0 (MPa)	Y_{Max} (MPa)	β (MPa)	n	G_T' (MPa·K^{-1})	G_P'	Y_P'	γ_0	C_0 (m·s^{-1})	S
5.234	280	27	410	126	0.15	−17.3	1.9	1.87×10^{-2}	2	5322	1.334

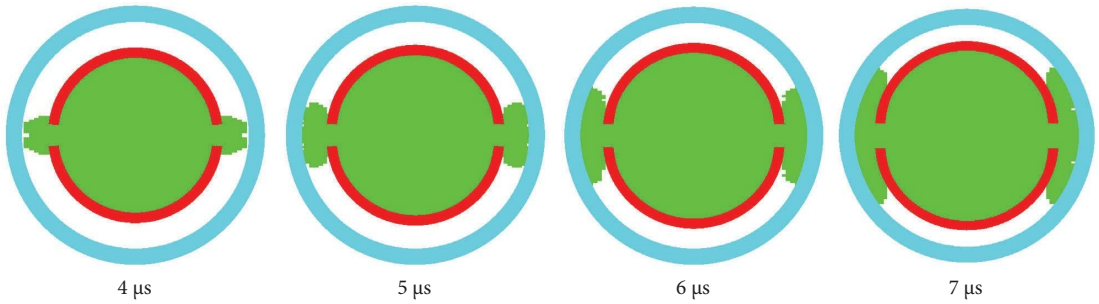

Figure 10: Detonation gas distribution for split-tube charge holders.

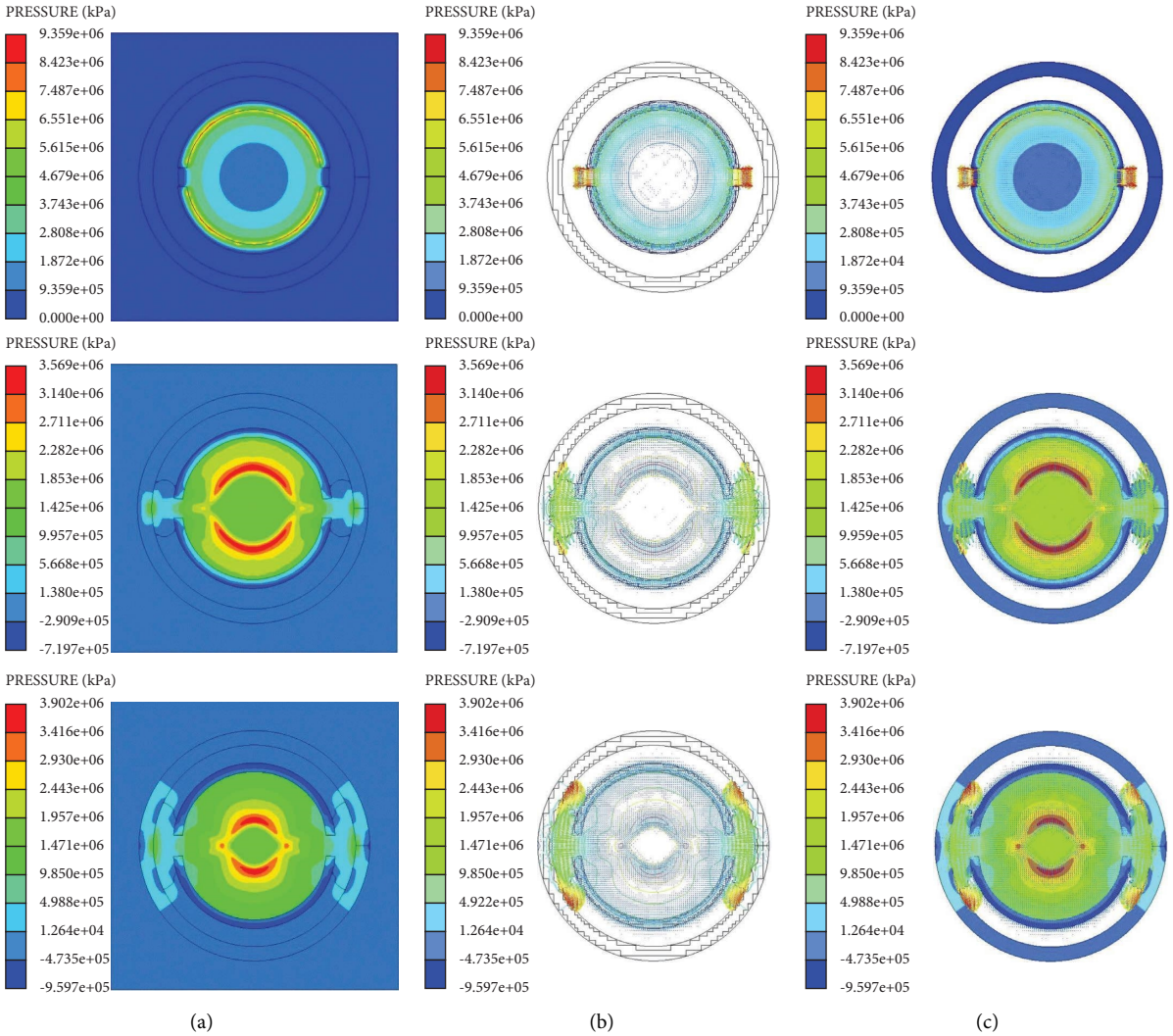

Figure 11: Explosion wave propagation of split-tube charge holder in the blast-hole. (a) Effective stress. (b) Pressure line. (c) Velocity vector.

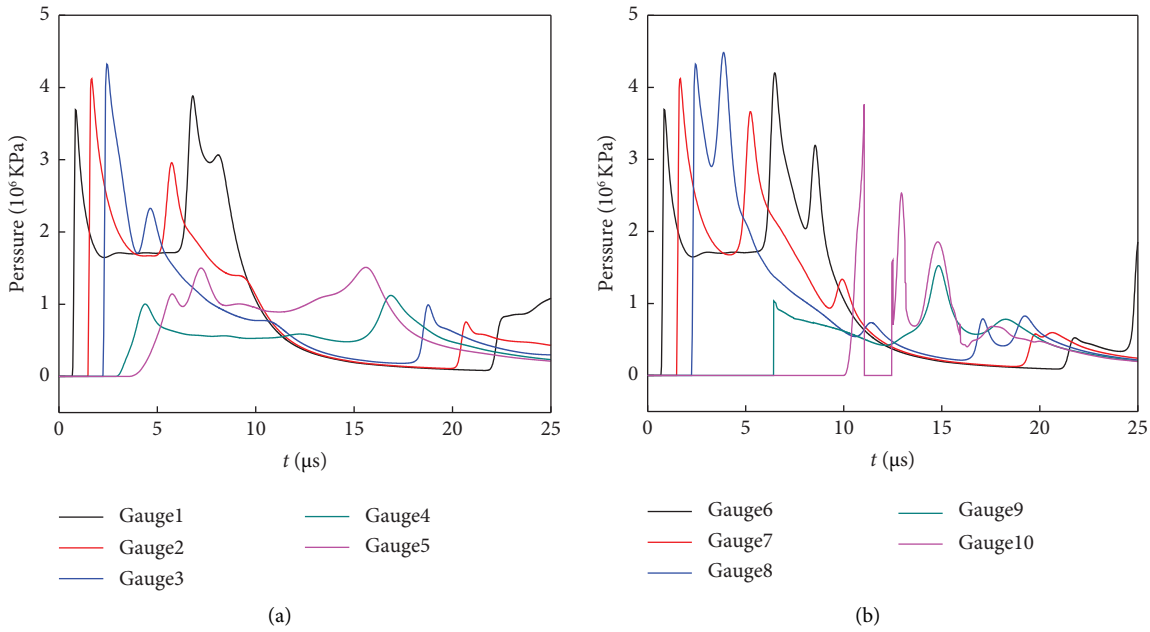

Figure 12: Pressure changes in blast-hole. (a) Cutting seam direction. (b) Vertical cutting seam direction.

5. Conclusion

The goal of this work was to capture the fine structural features of a cartridge explosion wave during propagation using the high-speed schlieren photography technique, and the following conclusions are obtained as follows:

(1) Compared with the common cartridge, the cutting seam cartridge can gather explosion gas, leading to expansion of the explosion gas in a specific direction, leading to enhanced damage to the medium in that direction.

(2) The explosion wave is reflected by the blast-hole wall, but the explosion gas reaches the blast-hole wall in an uneven manner without being significantly reflected. The cartridge explosion wave first travels in the slit direction, and the explosion gas expands in an linearly spread form along the slit direction.

(3) The explosion gas mainly impacts and gathers in the slit direction, and then travels around in other directions. The explosion wave propagates speeds is similar of two cartridges, however, the propagation speed of explosive gas in slit cartridge is significantly higher than that of ordinary cartridge.

(4) Numerical simulation results verified high speed schlieren experiment, the explosion wave first releases energy in the slit direction because initial damage to the blast-hole wall. Further damage to the damaged blast-hole wall occurs due to the quasi-static pressure of the high-pressure explosion gas.

Data Availability

The data used to support the findings of this study are available from the corresponding author upon request.

Conflicts of Interest

The authors declare that there are no conflicts of interest.

Acknowledgments

This research was supported by the National Natural Science Foundation of China (Nos. 52208384 and 51934001), the National Key Research and Development Program (2021YFB3401501), the State Key Laboratory of Precision Blasting and Hubei Key Laboratory of Blasting Engineering, and Jianghan University (No. PBSKL2022C05).

References

[1] W. L. Fourney, J. W. Dally, and D. C. Holloway, "Controlled blasting with ligamented charge holders," *International Journal of Rock Mechanics and Mining Sciences & Geomechanics Abstracts*, vol. 15, no. 3, pp. 121–129, 1978.

[2] W. L. Fourney, D. B. Barker, and D. C. Holloway, "Model studies of well stimulation using propellant charges," *International Journal of Rock Mechanics and Mining Sciences & Geomechanics Abstracts*, vol. 20, no. 2, pp. 91–101, 1983.

[3] S. H. Cho, Y. Nakamura, B. Mohanty, H. Yang, and K. Kaneko, "Numerical study of fracture plane control in laboratory-scale blasting," *Engineering Fracture Mechanics*, vol. 75, no. 13, pp. 3966–3984, 2008.

[4] A. L. Isakov, "Directed fracture of rocks by blasting," *Soviet Mining Science*, vol. 19, no. 6, pp. 479–488, 1983.

[5] P. Xu, R. S. Yang, Y. Guo, C. Chen, and Y. T. Zhang, "Experimental and numerical investigation of the interaction between blast wave and precrack in a defected material," *Applied Optics*, vol. 35, no. 58, pp. 9718–9727, 2019.

[6] W. Liu, Z. Yue, and G. Yang, "Experimental investigation of a circumferential crack in a PMMA cylindrical shell using caustics," *Polymer Testing*, vol. 79, Article ID 106086, 2019.

[7] R. S. Yang and J. J. Zuo, "Experimental research on explosively driven crack initiation and propagation from flaws of various

geometry," *Journal of Testing and Evaluation*, vol. 48, no. 2, p. 1154, Article ID 20170412, 2020.

[8] R. S. Yang, J. J. Zuo, Y. L. Li, Y. Zhao, and Y. Q. Kang, "Experimental study on slotted cartridge explosion wave propagation characteristic under different cutting seam pipe material," *Journal of China University of Mining and Technology*, vol. 48, no. 2, pp. 229–235, 2019.

[9] Z. W. Yue, P. Qiu, X. Wang, Y. Song, and Q. Yu, "Notched-borehole cut blasting study by the method of dynamic caustics," *Journal of China Coal Society*, vol. 41, no. 3, pp. 858–863, 2016.

[10] Z. W. Yue, Y. Guo, P. Xu, Q. Wan, and J. Y. Zhao, "Experimental study on the mechanism of blast-induced crack propagation under directional fracture controlled blasting," *Mechanical Engineering*, vol. 33, pp. 50–58, 2016.

[11] Z. W. Yue, L. Y. Yang, and Y. B. Wang, "Experimental study of crack propagation in polymethyl methacrylate material with double holes under the directional controlled blasting," *Fatigue and Fracture of Engineering Materials and Structures*, vol. 36, no. 8, pp. 827–833, 2013.

[12] D. M. Guo, K. Liu, H. Lu, R. Yang, C. Wang, and Y. Wang, "Fracture behavior of an empty hole using the digital laser dynamic caustic method under directional controlled blasting," *Materials Testing*, vol. 58, no. 11-12, pp. 982–991, 2016.

[13] R. S. Yang and Y. B. Wang, "Experimental research on the influence of an empty-hole defect on crack connections between a directionally fractured blast hole," *Journal of Testing and Evaluation*, vol. 45, pp. 2139–2150, 2017.

[14] Y. B. Wang, "Study of the dynamic fracture effect using slotted cartridge decoupling charge blasting," *International Journal of Rock Mechanics and Mining Sciences*, vol. 96, pp. 34–46, 2017.

[15] G. W. Ma and X. M. An, "Numerical simulation of blasting-induced rock fractures," *International Journal of Rock Mechanics and Mining Sciences*, vol. 45, no. 6, pp. 966–975, 2008.

[16] A. Hanenkamp and W. Merzkirch, "Investigation of the properties of a sharp-focusing schlieren system by means of Fourier analysis," *Optics and Lasers in Engineering*, vol. 44, no. 3-4, pp. 159–169, 2006.

[17] F. Sourgen, F. Leopold, and D. Klatt, "Reconstruction of the density field using the colored background oriented schlieren technique (CBOS)," *Optics and Lasers in Engineering*, vol. 50, no. 1, pp. 29–38, 2012.

[18] R. S. Yang, J. J. Zuo, and G. L. Yang, "An experimental study on slotted cartridge directional controlled blasting," *Journal of Vibration and Shock*, vol. 37, no. 24, pp. 24–29, 2018.

[19] R. S. Yang and J. J. Zuo, "Experimental study on directional fracture blasting of cutting seam cartridge," *Shock and Vibration*, 2019.

[20] J. J. Zuo, R. S. Yang, X. Ma, L. Y. Yang, and Y. Zhao, "Explosion wave and explosion fracture characteristics of cylindrical charges," *International Journal of Rock Mechanics and Mining Sciences*, vol. 135, Article ID 104501, 2020.

[21] D. Ambrosini and G. Rajshekhar, "Multi-scale approach for analyzing convective heat transfer flow in background-oriented Schlieren technique," *Optics and Lasers in Engineering*, vol. 110, pp. 415–419, 2018.

[22] D. Ambrosini, D. Paoletti, R. Di Biase, P. K. Rastogi, and S. Siva Gorthi, "Role of data processing in measuring temperature gradients with DOE Schardin's schlieren #2," *Optics and Lasers in Engineering*, vol. 50, no. 8, pp. 1069–1074, 2012.

[23] G. Zhang, "Experimental study on shock wave propagation of the explosion in a pipe with holes by high-speed schlieren method," *Shock and Vibration*, vol. 2020, Article ID 8850443, 9 pages, 2020.

[24] Y. Ju, C. D. Xi, Y. Zhang, L. T. Mao, F. Gao, and H. P. Xie, "Laboratory in situ ct observation of the evolution of 3D fracture networks in coal subjected to confining pressures and axial compressive loads: a novel approach," *Rock Mechanics and Rock Engineering*, vol. 51, no. 11, pp. 3361–3375, 2018.

[25] X. Liu and L. S. Liu, "An immersed transitional interface finite element method for fluid interacting with rigid/deformable solid," *Engineering Applications of Computational Fluid Mechanics*, vol. 13, no. 1, pp. 337–358, 2019.

[26] P. C. Souers and R. Minich, "Cylinder test correction for copper work hardening and spall," *Propellants, Explosives, Pyrotechnics*, vol. 40, no. 2, pp. 238–245, 2015.

[27] L. Chen, R. Li, and C. B. Yao, "An Approximate Riemann solver for fluid-solid interaction problems with mie-gruneisen equations of state," *Communications in Computational Physics*, vol. 27, no. 3, pp. 861–896, 2020.